



Review

# Review of Photovoltaic–Battery Energy Storage Systems for Grid-Forming Operation

Kai Yin, Yi Xiao, Xiaomeng Shen, Yinxiao Zhu and Yongheng Yang \*

College of Electrical Engineering, Zhejiang University, Hangzhou 310027, China; kai\_yin@zju.edu.cn (K.Y.); yi\_xiao@zju.edu.cn (Y.X.); xiaomeng.shen@zju.edu.cn (X.S.); yinxiao.zhu@zju.edu.cn (Y.Z.)

\* Correspondence: yoy@zju.edu.cn

**Abstract:** Coordinated control technology attracts increasing attention to the photovoltaic–battery energy storage (PV-BES) systems for the grid-forming (GFM) operation. However, there is an absence of a unified perspective that reviews the coordinated GFM control for PV-BES systems based on different system configurations. This paper aims to fill the gap by providing a comprehensive review of coordinated GFM control strategies for PV-BES, considering various system configurations. Typical configurations of PV-BES systems are explored, followed by a detailed discussion of conventional GFM control methods used in the PV-BES systems. Furthermore, coordinated GFM controls are analyzed in PV-BES systems based on different configurations, providing the common DC bus configuration as a widely adopted configuration due to its more control degrees of freedom and ease of expansion. Moreover, the mode division and switching coordinated control based on the system power is the most widely used. Furthermore, challenges in the coordinated GFM controls for the PV-BES system in future applications are briefed and emphasized before the conclusion.

**Keywords:** photovoltaic; battery energy storage; grid-forming control; frequency support; coordinated control



**Citation:** Yin, K.; Xiao, Y.; Shen, X.; Zhu, Y.; Yang, Y. Review of Photovoltaic–Battery Energy Storage Systems for Grid-Forming Operation. *Batteries* **2024**, *10*, 288. <https://doi.org/10.3390/batteries10080288>

Academic Editors: Carlos Ziebert and Rodolfo Dufo-López

Received: 14 June 2024

Revised: 21 July 2024

Accepted: 9 August 2024

Published: 12 August 2024



**Copyright:** © 2024 by the authors. Licensee MDPI, Basel, Switzerland. This article is an open access article distributed under the terms and conditions of the Creative Commons Attribution (CC BY) license (<https://creativecommons.org/licenses/by/4.0/>).

## 1. Introduction

In recent years, high penetration of renewable energy sources (RESs), such as photovoltaic (PV) energy, has gained increasing attention considering the environmental concerns [1]. Conventionally, the interface between the PV generation and the grid is power electronics equipment. Therefore, the power system is gradually shifting from a synchronous-generators-based system to a power-electronics-based system, as shown in Figure 1 [2–5]. Unlike synchronous generators (SGs), the power electronics equipment lacks inherent inertia, degrading the power system's stability.

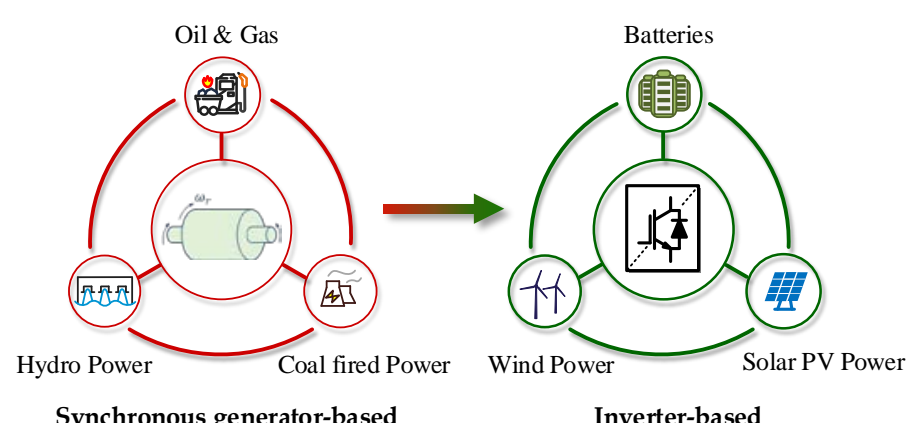


**Figure 1.** Power system shifting from a synchronous generator-based to an inverter-based system.

Subsequently, the grid-forming (GFM) control has become an emerging solution for frequency and voltage support. However, extra energy is needed in the GFM control to participate in the frequency regulation [6–8]. Typically, the PV system operates at the maximum power point (MPP) without reserving spare energy. In order to provide energy for inertia support and frequency regulation, a battery energy storage (BES) system is commonly integrated into the PV system [9]. Conventionally, the BES is integrated on the AC or DC sides in the PV-BES-GFM system. Basically, the common AC bus configuration is a simple solution for BES integration with superior scalability [10]. However, the multiple conversion stage in common AC bus architecture induces adverse power losses and degrades the system efficiency. Alternatively, the BES can be connected with the common DC bus through the bidirectional DC-DC converters directly, extending the control degrees of freedom (DoFs) [11]. Moreover, the direct connection reduces the sophisticated conversion stages and enhances system efficiency. Unlike the aforementioned architecture, three-port converters (TPCs) exhibit advances in control flexibility and single-stage power conversion, guaranteeing the simplicity, reliability, and efficiency of the system [12]. Compared with conventional common AC/DC architectures, the TPC-based integration may raise concerns about complexity of the control and scalability of the system [13].

Conventionally, the synchronization of the grid following (GFL) control is dependent on the grid information, facing the instability risk induced by the increasing proportion of the low inertia PV integration [4]. Accordingly, the GFM control is proposed to establish a stable frequency and voltage to provide frequency and voltage support to the grid. The application of GFM controls in power systems is underscored in [14], which also identifies the challenges associated with high overcurrent and techniques required to prevent overloading. Ref. [15] started by outlining the requirements for inverter-based resources and provided a comprehensive review of grid-forming control strategies. Ref. [16] provided a comprehensive review of existing control methods for GFM converters in grid-connected applications, offering a comparative analysis of grid support capabilities and typical applications. However, these reviews lack a unified control structure for grid-forming control, which is addressed in [17]. A generalized control framework for the GFM inverter is established according to the different GFM control functions.

Droop control is the most common GFM control, which mimics the droop characteristics of SGs to regulate the frequency [7]. However, the droop control lacks inertia support capability. The virtual synchronous generator (VSG) control has been explored to emulate the SGs swing equations to provide inertia and voltage support to the grid [8]. Moreover, since the physical DC-link capacitor can be equivalent to the rotor energy storage of SGs, the matching control is proposed to synchronize with the grid by the DC-link voltage [18]. It should be mentioned that a variation in the DC-link voltage constitutes a risk to the power system. Furthermore, the virtual oscillator control (VOC) has been recognized as a viable option in the GFM control, which is a nonlinear control strategy derived from the inherent synchronization characteristics of the oscillators [19]. The VOC enables the converters to synchronize with each other at indeterminate initial states without power calculations and communications. However, complex control algorithms need to be considered in the VOC, which pose considerable technical challenges in applications, requiring further simplification and optimization [20].

Existing reviews of the PV-BES-GFM system mainly focus on planning and operation scheduling, system structures, and efficiency. Ref. [21] demonstrated the investment decision, optimal sizing, and operation scheduling of the PV-BES system, which revealed the aspects needed to be considered when installing a PV-BES system. A detailed plan for the charging and discharging of the BES is suggested to optimize battery capacity in the PV-BES system [22]. Furthermore, the BES response speed is crucial for the PV-BES-GFM operation. Control strategies have been proposed to improve the DC-link voltage dynamics [23]. Additionally, typical PV-BES system structures are compared based on the total components, voltage conversation ratio, and system efficiency [24]. It should be mentioned that the configuration of the PV-BES system is crucial for coordinated control, enabling

effective power management and frequency regulation [25]. The configuration determines the coordinated control for power flow, mode division, and switching within the PV-BES system [26]. In the common DC bus configuration, the BES system is directly connected to the common DC bus via bidirectional DC-DC converters. The power flow characteristics in a common DC bus configuration differ from common AC bus configuration, leading to variations in the mode division and switching methods required for the coordinated GFM control of PV-BES systems. Additionally, the common DC bus configuration, with its increased control degrees of freedom, provides greater opportunities for improving power balancing and frequency regulation performance [27]. Regarding the coordinated control of the PV-BES system for GFM operation, there is a notable gap in the existing review literature. Current reviews on PV-BES systems predominantly emphasize the types of energy storage, control methods for PV and storage, and the configurations of PV-BES systems [28–30]. However, there is a lack of a unified perspective that reviews the coordinated GFM control of PV-BES systems based on different system configurations. This paper aims to address the gap by providing a comprehensive review of coordinated GFM control strategies for PV-BES, considering various system configurations.

Aiming to investigate the PV-BES GFM coordinated control based on the different structures, this paper carries out an overview of the structures and controls of the PV-BES systems towards the GFM operation. The rest of the paper is organized as follows. The structures of the PV-BES system are introduced and compared in Section 2. Typical GFM controls are presented in Section 3. In Section 4, the coordinated control of the PV-BES system is explored and highlighted, where the parameter design is of importance, as emphasized. Finally, concluding remarks are provided in Section 5.

## 2. Typical Configuration of the PV-BES System

It should be mentioned that the typical configuration of the PV-BES-GFM system includes the common AC bus connection [11], the common DC bus connection [10], and the TPCs [12,13]. When selecting the system configuration, it is necessary to consider aspects such as the scalability of the configuration, efficiency, system control degrees, and cost [31–36].

The common AC-bus connection for the PV-BES-GFM system is shown in Figure 2, where the PV system and the BES are both connected to the AC bus. The PV panels are interfaced with a DC-DC converter, and the output of the PV power is linked to a DC-AC inverter. The BES is connected to the AC bus through a DC-AC inverter [31,32]. It should be noted that the integration of the BES does not impact the existing PV system with scalability. However, due to the configuration limitations, the BES can only absorb the power from the AC bus, and the PV power needs a multi-stage to reach the BES, which causes low efficiency in the PV-BES-GFM system. Furthermore, the integration of the PV system and the BES at the AC bus leads to a decrease in the control degrees of freedom [33].

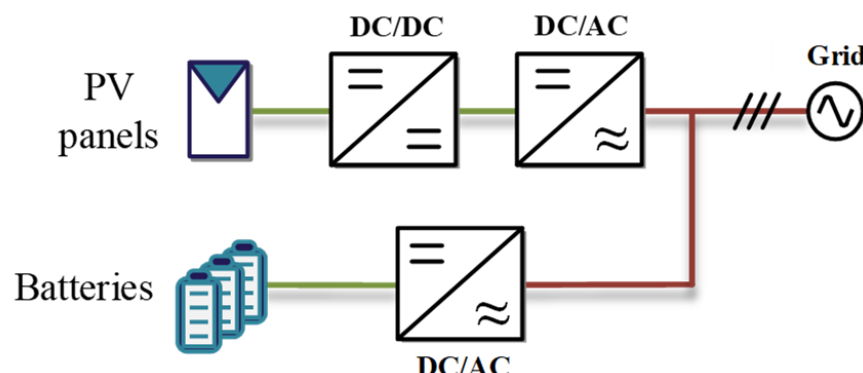


**Figure 2.** Common AC bus connection of the PV-BES-GFM system (the red line represents AC currents, and the green line represents the DC currents).

A common DC bus connection in the PV-BES-GFM system is proposed to address these issues [36]. Figure 3 illustrates the configuration of the common DC bus connection in the PV-BES-GFM system. Both the PV system and the BES are connected to the DC bus through the capacitor, jointly supplying energy to the grid. It is noteworthy that a bi-directional DC-DC converter plays an essential role in the BES. It facilitates the management of the BES charge and discharge process, along with the DC-link voltage control. A description of bidirectional DC-DC converters will be introduced later. Compared with the common AC bus connection, control degrees of freedom in the common DC bus connection are increased. The PV power can charge the battery directly through the DC bus, which increases efficiency. Furthermore, employing fewer inverters in the common DC bus connection makes it more economical. Compared with other connections, the common DC bus connection is widely used in the PV-BES-GFM system due to its low cost and simplicity for coordinated controls [37]. Nevertheless, the operation of the PV system and the BES are tightly interconnected with the DC bus, indicating that any malfunction in the DC-link voltage would impact both the PV system and the BES [38].

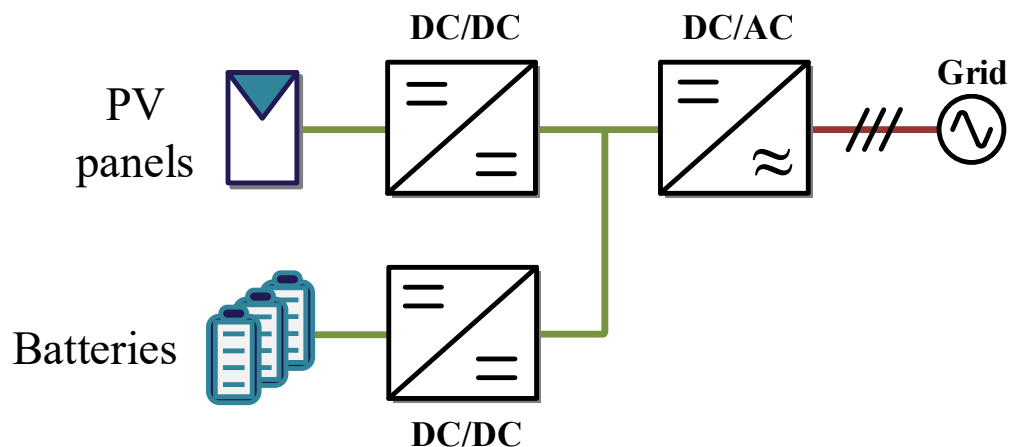


**Figure 3.** Common DC-bus connection of the PV-BES-GFM system (the red line represents AC currents, and the green line represents the DC currents).

Additionally, the bi-directional DC-DC converter is the interface between the BES and the DC bus, as illustrated in Figure 4 [39]. Typical bi-directional DC-DC converters include bi-directional boost converters, bi-directional LLC resonant converters, and dual active bridge DC-DC converters (DAB) [40–42]. As shown in Figure 4a, the bi-directional boost converter topology and control strategy are relatively simple. However, due to the inherent structure limitations, the power conversion efficiency is relatively low. When there is a need for high power and electrical isolation occasions, the bi-directional LLC resonant converter emerges as a preferred option. It is a kind of converters based on an LLC resonant circuit, as shown in Figure 4b. However, the voltage gain during the reverse operation mode is relatively low, which may fail to meet the PV-BES-GFM system voltage requirements [42]. An auxiliary inductor is added to increase the voltage gain during reverse mode at the midpoint of the full bridge [43]. Despite increasing the voltage in the reverse mode, the extra introduction of inductor causes more loss. This issue can be avoided in the DAB converter, as shown in Figure 4c. Moreover, zero voltage switch (ZVS) of switching devices can be realized in the DAB, reducing the switching loss and avoiding electromagnetic interference [44–46].

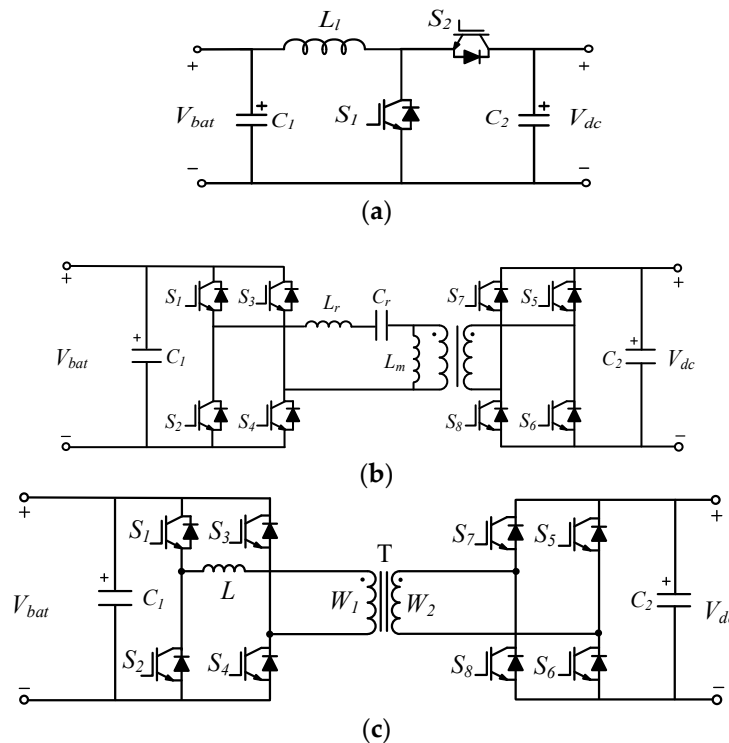


**Figure 4.** Typical bidirectional power converters for BES systems: (a) bi-directional boost converter; (b) bi-directional LLC resonant converter; (c) dual active bridge DC-DC converter.

However, it should be emphasized that both the common AC and DC bus connections are integrated into the grid with a shared AC/DC bus, which is a multi-stage conversion. The TPCs integrate DC-DC converters to enhance the system efficiency as a single-stage power conversion, as shown in Figure 5. Typical TPCs include the Z-source converter (ZSC) and interlinking source converters [12,47–49], as depicted in Figure 6. A shoot-through (ST) state is applied in the ZSC, enabling the converter to achieve both boost and invert functions in a single-stage system. However, the range of the output voltage is limited. To address this issue, the ZSC is improved by introducing a boost circuit to provide a greater voltage gain [50,51], called Quasi-Z-source inverter (QZSI), as shown in Figure 6a, whereas the PV-BES-GFM system fails to support the grid when solar irradiance is low, which requires special control to avoid. Moreover, the structure is highly integrated with poor scalability. Moreover, controlling the QZSI in the PV-BES-GFM system tends to be more challenging due to less control degrees of freedom and complex power flow [52,53]. The interlinking converter is also presented for single-stage power conversion in the PV-BES-GFM system [54–56], which enables flexible integration of the PV system and BES into the grid, as shown in Figure 6b. It is a kind of modified boost topology where the switch devices are substituted with converters. However, more switch devices are needed in the interlinking converter, which causes lower efficiency compared to the QZSI [57,58]. The comparison of the typical structures for the PV-BES-GFM system are concluded in Table 1.

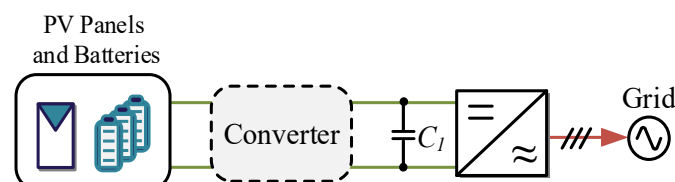


**Figure 5.** Integration of PV panels and batteries into the grid with a single-stage power conversion (using advanced power converters, e.g., multiport converters; the red line represents AC currents, and the green line represents the DC currents).

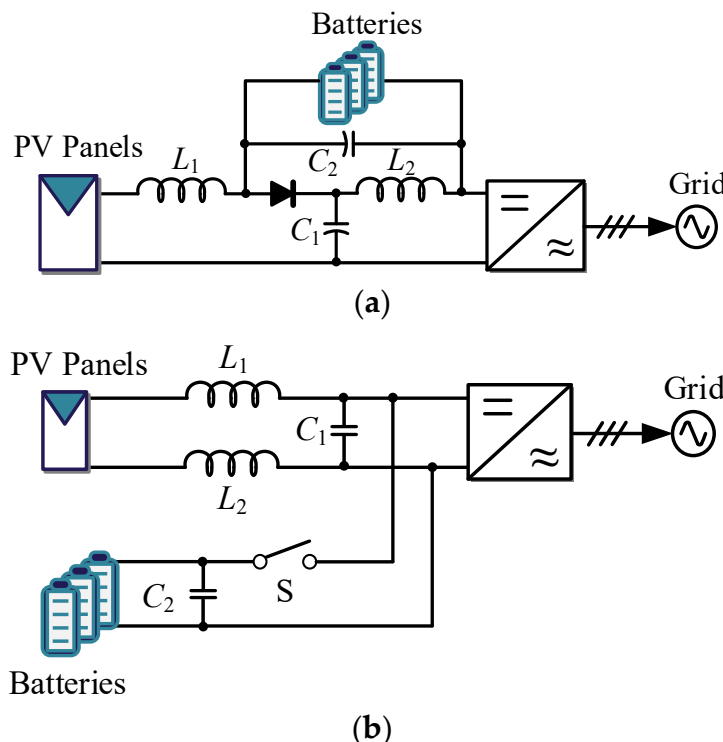


**Figure 6.** Examples of PV-BES systems: (a) PV-BES system with Z-source inverters; (b) PV-BES system with interlinking converter.

**Table 1.** Comparison of the PV-BES-GFM system configuration.

Configuration	Common AC-Bus	Common DC-Bus	TPCs
Structure scalability	Easy	Difficult	Difficult
Control degrees	Less	More	More
Efficiency	PV to batteries	Low	High
	PV to the grid	High	Low
	Batteries to the grid	High	High
Cost	High	Low	Highest

### 3. Typical GFM Controls in PV-BES System

The control structure for the grid-connected inverters can be categorized into GFL and GFM schemes. The GFL control cannot provide frequency and inertia support to the grid, which regulates the injected current to the grid and relies on stable grid voltage to achieve synchronization. Enhanced GFL control methods have been proposed to improve the frequency response, such as current-controlled droop control and current-controlled virtual synchronous generator (VSG) control [59,60]. However, these improved controls also deteriorate the stability of grid-connected converters under weak grids. Considering the issues of the GFL control in the power system, the GFM control has become an emerging technology due to the constant output voltage and frequency. The GFM control is initially designed as a constant voltage/frequency ( $V-f$ ) control, which operates as an ideal voltage source to form the PCC voltage [61].

A typical structure of the GFM control used in the PV-BES-GFM system is illustrated in Figure 7 [33,62]. It consists of three parts: the PVS, the BESS, and the grid-connected inverter. The PV system and the BESS are linked to the DC-link through the capacitor  $C_{dc}$ , jointly supplying energy to the inverter as the primary source. The inverter is connected to the grid through a filter. Here,  $C_{dc}$  represents the DC-link capacitor.  $L_f$  and  $R_f$  represent the inductance and resistance of the filter, respectively.  $Z_g$  and  $V_g$  represent the impedance

and voltage amplitude of the grid, respectively.  $V_o$  and  $i_o$  represent the voltages and the currents of the PCC, respectively.  $P_e$  and  $Q_e$  are the active and reactive power of the inverter. The GFM control generates voltage reference  $V_{ref}$  and phase angle reference  $\theta_{ref}$  to the inner control loop, which is used to regulate the output voltage. Typical GFM controls include droop control, virtual synchronous control (VSG), matching control, and virtual oscillating control (VOC), which difference lies in the methods of generating reference voltage, as shown in Figure 8. The typical GFM controls in PV-BES system will be described in the following.

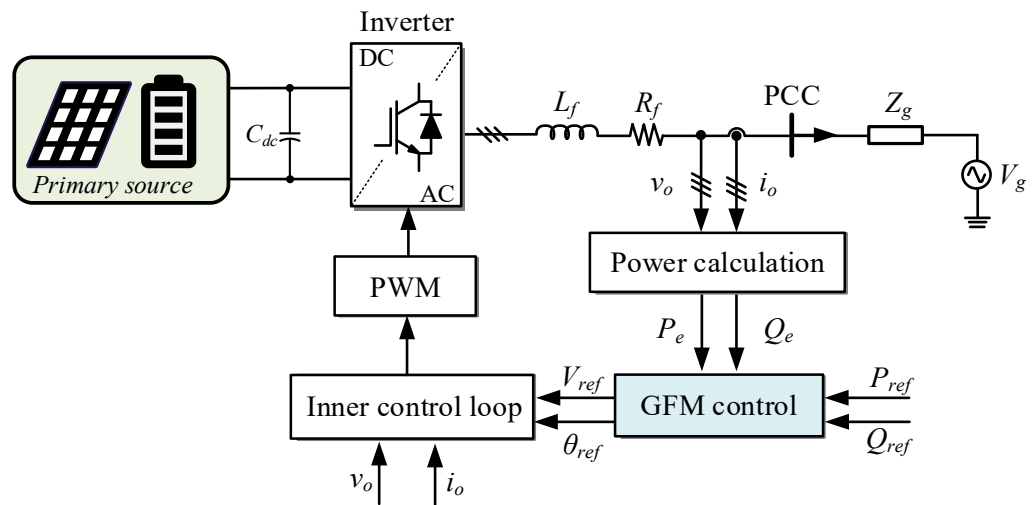


**Figure 7.** Typical control structure of the PV-BES system with the GFM control (PWM: pulse width modulation; PCC: point of common coupling;  $v_o$ : voltages of the PCC;  $i_o$ : currents of the PCC;  $P_e$ : active power of the inverter;  $Q_e$ : reactive power of the inverter;  $P_{ref}$ : active power reference;  $Q_{ref}$ : reactive power reference).

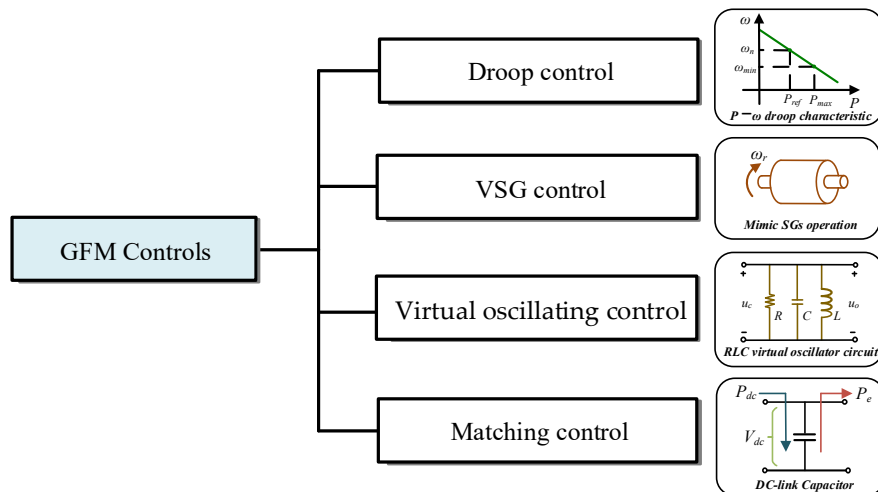


**Figure 8.** GFM control schemes used in the PV-BES system.

### 3.1. Droop Control

Droop control mimics the droop characteristics of the SGs, regulating the output voltage and frequency of the inverter, which can be described as [63]

$$\omega_{ref} = \omega_n + k_p(P_{ref} - P_e), \quad (1)$$

$$V_{ref} = V_n + k_q(Q_{ref} - Q_e), \quad (2)$$

where  $k_p$  and  $k_q$  represent the active power droop coefficient and reactive power droop coefficient, respectively.  $P_{ref}$  and  $Q_{ref}$  represent active power and reactive power reference, respectively.  $\Omega_n$  and  $V_n$  are the rated angular frequency and PCC voltage.

The characteristics of the droop control and control block diagram are shown in Figures 9 and 10, respectively. The phase angle reference and the reference voltage of the inverter are generated according to the droop characteristic. By regulating the output frequency and voltage of the inverter, the droop control can respond to the power changes rapidly. Here,  $k_p$  and  $k_q$  are used to regulate the active power and reactive power, which are usually determined by the regulations of the transmission system operator (TSO). The droop control is relatively simple and easy to realize. However, the system is regulated only by the constant proportional gain and cannot provide inertia support to the power system. Therefore, adaptive droop control is proposed in [64], which replaces the active power droop coefficient and reactive power droop coefficient from a constant to an alterable one. And the droop control is based on local measurements, eliminating the need for complex and costly communication infrastructure. It enables automatic load sharing among different generation units, ensuring that each unit shares the load according to its capacity. The inherent limitations of the conventional droop control scheme are revealed in [65,66]. The control strategy struggles with accurate proportional load sharing due to the stringent requirements of identical per-unit impedance and voltage set-points for parallel-operated inverters, which are difficult to achieve. In addition, the inertia can be added to the droop control by adopting a low pass filter (LPF) for the active power and reactive power control loops [67].

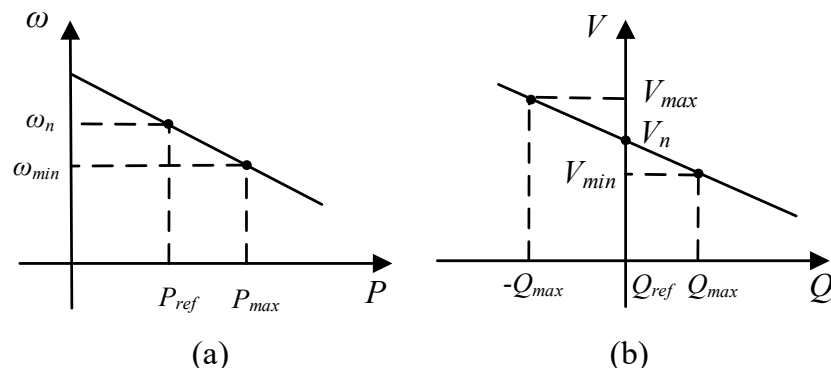


**Figure 9.** Characteristics of droop control: (a)  $P-\omega$  droop; (b)  $Q-V$  droop.

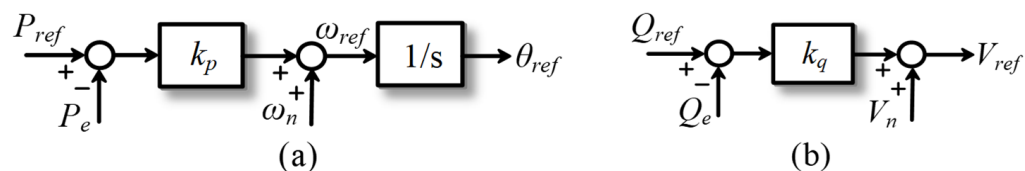


**Figure 10.** Control block diagram of the droop control: (a)  $P-\omega$  droop; (b)  $Q-V$  droop.

### 3.2. Virtual Synchronous Generator Control

The virtual synchronous generator (VSG) control has been explored to emulate the SGs swing equations to provide inertia and voltage support to the grid. Typically, the active power control and reactive control are involved in the VSG control [68], which are shown in Figure 11. Mostly, the VSG active power control loop simulates SGs swing equation, which can be described as

$$J\omega_n \frac{d\omega}{dt} = P_{ref} - P_e + D_p(\omega - \omega_n), \quad (3)$$

with  $J$  and  $D_p$  representing the moment of inertia and the damping coefficient, respectively. The VSG active power control loop is shown in Figure 11a.  $D_p(\omega - \omega_n)$  is adopted to

emulate the damping winding of the SGs, providing dampness to the power system. With proper energy storage, the VSG inverter provides frequency support to the grid [69]. The VSG control provides virtual inertia, mitigating the low inertia issues associated with high penetration of PV generation and enhancing dynamic response capabilities. However, it should be mentioned that improper selection of VSG control parameters can easily cause oscillations in active power. Consequently, the control parameters require precise tuning. An alternating moment of inertia is elaborated in [70] via transient energy analysis. However, a unified method for VSG control parameter design was not provided. Following the analysis of the small signal stability of the VSG control, a method for designing optimal controller parameters is proposed [71]. Moreover, virtual synchronous generators are limited by the over-current characteristics of power electronic devices, preventing them from supporting large short-circuit currents.

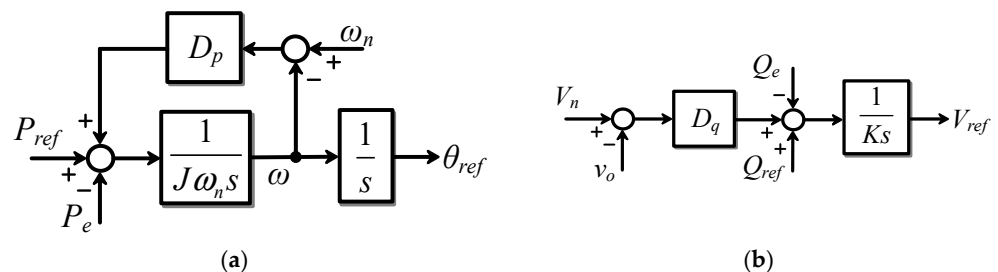


**Figure 11.** Power control loops of the virtual synchronous generator (VSG) control: (a) active power control loop; (b) reactive power control loop.

Moreover, the reactive power control can be described as

$$V_{ref} = \frac{1}{K_s} [D_q(V_n - V_o) + (Q_{ref} - Q_e)], \quad (4)$$

where  $V_o$  and  $D_q$  represent the PCC voltage amplitude and the reactive power droop coefficient, respectively.  $K$  represents the inertia coefficient of the reactive power control loop. Therefore, the VSG reactive power control loop regulates grid voltage by changing the reactive power, as shown in Figure 11b.

### 3.3. Virtual Oscillator Control

The virtual oscillator control (VOC) has been recognized as a viable option in the GFM control, which is a nonlinear control strategy derived from the inherent synchronization characteristics of the oscillators [71–73]. More recently, the dispatchable virtual oscillator control (dVOC) has been increasingly adopted to encompass all oscillator-based control strategies [20].

The simplified circuit diagram of the dVOC are presented in Figure 12.  $u_C$  and  $i_L$  represent the voltage of the virtual capacitor  $C$  and the current of the virtual inductor  $L$ , respectively.  $k_i$  and  $k_v$  represent the current gain and voltage gain, respectively.  $i_\alpha$  and  $i_\beta$  are the currents of the PCC in the  $\alpha$ - $\beta$  frame.  $v_{\alpha ref}$  and  $v_{\beta ref}$  represent a pair of orthogonal voltages gained by the output state variables from a virtual RLC circuit, respectively. The state variables  $x_1$  and  $x_2$  can be expressed as

$$\begin{cases} x_1 = u_C (\varepsilon = \sqrt{L/C}), \\ x_2 = \varepsilon i_L \end{cases}, \quad (5)$$

where  $f(x_1, x_2)$  is the function of the nonlinear oscillators determined by the state variables [74].

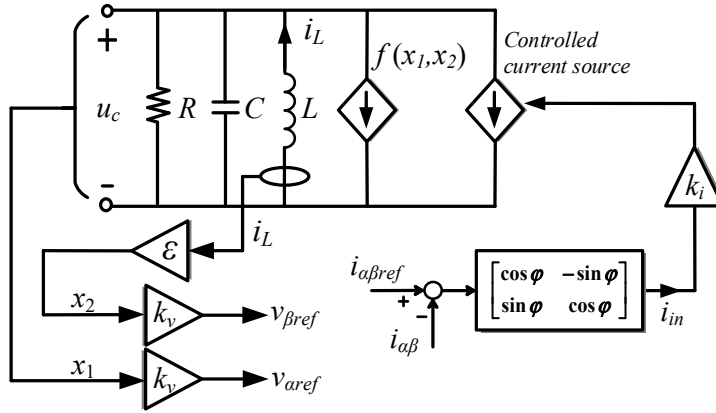


**Figure 12.** Circuit diagram of the dispatchable virtual oscillator control (dVOC).

As shown in Figure 12, the reference currents  $i_{\alpha ref}$  and  $i_{\beta ref}$  are derived from the active and reactive power reference, which can be calculated as

$$\begin{bmatrix} i_{\alpha ref} \\ i_{\beta ref} \end{bmatrix} = \frac{2}{3|v_{\alpha\beta}|^2} \begin{bmatrix} v_{\alpha ref} & v_{\beta ref} \\ v_{\beta ref} & -v_{\alpha ref} \end{bmatrix} \begin{bmatrix} P_{ref} \\ Q_{ref} \end{bmatrix}. \quad (6)$$

After rotation matrix  $R(\varphi)$ , the input current acted as a controlled current source in the virtual RLC circuit, which can be described as

$$R(\varphi) = \begin{bmatrix} \cos \varphi & -\sin \varphi \\ \sin \varphi & \cos \varphi \end{bmatrix}. \quad (7)$$

Usually,  $\varphi = \pi/2$  or  $\varphi = 0$  is desirable. Furthermore, the phase angle reference for the  $dq$  transformation can be calculated as  $\theta = \tan^{-1}(v_\beta/v_\alpha)$  to the inner control loop. The VOC exhibits robust adaptability in response to variable grid conditions. It enables converters to achieve synchronization from indeterminate initial states without power calculations or communication [75]. A fuzzy-based adaptive VOC method is proposed in [76] to maintain the output voltage. Moreover, the model and stability of the VOC are proposed in [73]. However, the development of the VOC is still in a relatively nascent stage. Complex control algorithms need to be considered in the VOC, which pose considerable technical challenges in applications, requiring further simplification and optimization.

### 3.4. Matching Control

Since the physical DC-link capacitor can be equivalent to the rotor energy storage of SGs, matching control is proposed to synchronize with the grid by the DC-link voltage, which provides the phase angle reference  $\theta_{ref}$  to the inner control loop [77]. The matching control can be described as

$$\omega = \omega_n + G(s) \cdot (V_{dc ref} - v_{dc}), \quad (8)$$

where the  $V_{dc ref}$  and  $v_{dc}$  represent the DC-link voltage reference and DC-link voltage, respectively. The  $G(s)$  is a transfer function, which can be a proportional (P) controller or a proportional integral (PI) controller. The DC-link voltage  $v_{dc}$  reflects the power difference between the DC-side and AC-side, which acts like frequency  $f$ . The block diagram of matching control is presented in Figure 13 [78,79]. However, the matching control only provides  $\theta_{ref}$  to the inner control loop. The  $V_{ref}$  for the PCC voltage is regulated by the reactive power control loop, as shown in Figure 11. As shown in Figure 13, the matching control operates on the error  $V_{dc ref} - v_{dc}$  and the dynamics of the closed loop are influenced by the operating point,  $v_{dc0}$ . This inconvenience can be avoided by replacing the  $V_{dc ref} - v_{dc}$  with  $\frac{1}{2} \left[ (V_{dc ref})^2 - (v_{dc})^2 \right]$ , which is related to the DC capacitor energy [80]. Moreover,

certain high-frequency noise signals can also be eliminated. The advantage of matching control lies in its superior capability to regulate DC-link voltage compared to other GFM controls. However, it fails to maintain a constant voltage value [79]. Additionally, this control strategy requires adequate DC capacitor capacity. The comparison of the typical GFM controls is concluded in Table 2.

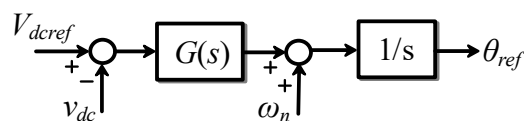


**Figure 13.** Control block diagram of the matching control (using DC-link dynamics to emulate the feature of the synchronous generator).

**Table 2.** Comparison of the typical GFM controls in PV-BES-GFM system.

GFM Control	Advantages		Disadvantages	
Droop control	(1) Easy to realize. (2) Automatic load sharing among different generation units.		(1) Lack of inertia support capability. (2) Sensitivity to parameter settings.	
VSG control	(1) Inertia support. (2) Enhancing the control system dynamic response capabilities.		(1) Requiring precise parameter tuning. (2) Inherent oscillation characteristics.	
VOC control	(1) Strong adaptability. (2) Fast response speed. (3) Synchronize without the need for power calculations.		(1) Lower technology maturity. (2) Less effective in power control. (3) Complex control algorithms.	
Matching control	(1) More flexibility. (2) DC voltage can be regulated.		(1) Higher failure risk. (2) Adequate DC capacitor capacity.	

#### 4. Coordinated Control of the PV-BES System

It is important to note that GFM controls rely on the unpredictable grid power demand, which requires effective management of the power flow between the PV system, the BES, and the grid, as well as providing frequency support within the PV-BES system. The configuration of the PV-BES system is crucial for coordinated control, enabling effective power management and frequency regulation, which determines the coordinated control for power flow, mode division, and switching. The detailed coordinated controls based on different configurations in the PV-BES system will be elaborated in the following.

##### 4.1. Unified Mode Division and Switching Method

The mode division in coordinated control can be determined by factors that include the battery state of charge (SOC), PV system power, and grid power demand in any PV-BES configuration. These factors can be easily obtained in any configurations and fundamentally characterize the operating state of the PV-BES-GFM system.

Coordinated GFM control of PV and BES with mode division based on power and state of charge (SOC) was proposed in [81,82]. The inverter is regulated by the droop control, which supports the grid voltage and frequency when the primary source is adequate. The PV system always operates at the maximum power point (MPP), which extracts the maximum power to the grid. As shown in Figure 14, the control strategy assesses the power difference between the PV and grid power demand. If there is a surplus of PV power, the BES system needs to consume it. However, due to the physical properties of the battery, it only absorbs energy when the SOC is below  $SOC_{max}$ . Otherwise, the PV system is disconnected to prevent overcharging. The batteries then supply power to the grid independently. As the batteries discharge, the SOC will eventually fall below  $SOC_{max}$ , allowing the PV system to reconnect and charge the batteries. However, this control strategy results in significant power wastage while the PV system disconnects and the batteries supply power to the grid independently.

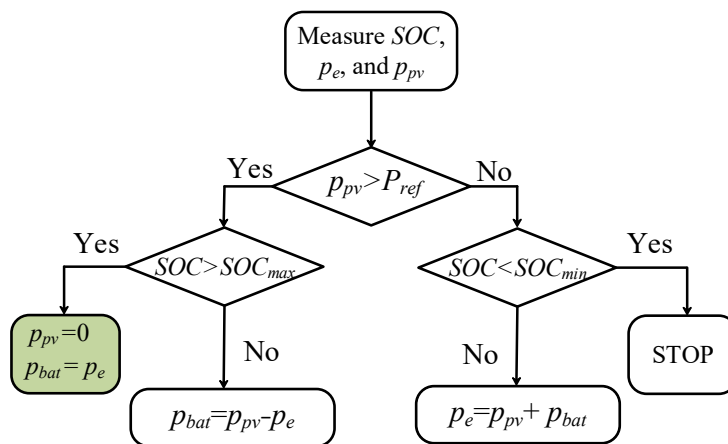


**Figure 14.** Coordinated control I for mode division and switching (PV system always works at MPP).

To utilize the PV power fully, the coordinated control II is proposed [83–85], which is similar to the control I, as illustrated in Figure 15. The difference between coordinated control I and coordinated control II lies in the PV control strategy when SOC is above the  $SOC_{max}$ . In coordinated control I, the PV system is disconnected to avoid over-charging the batteries, and the batteries provide energy to the grid independently. It wastes a lot of power. However, the PV system operates at reduced power to match the grid demand ( $p_{pv} = P_{ref}$ ) in coordinated control II. And the battery is disconnected to avoid overcharging. In addition, to extend the service life of batteries, a more detailed SOC control strategy is proposed in [86], which is segmented into five parts. Each segment sets a different current limitation for the battery to avoid the adverse impact of excessive current. Although this control method benefits battery health, it is too complex to implement coordinated control in the PV-BES-GFM system due to the current limitations.

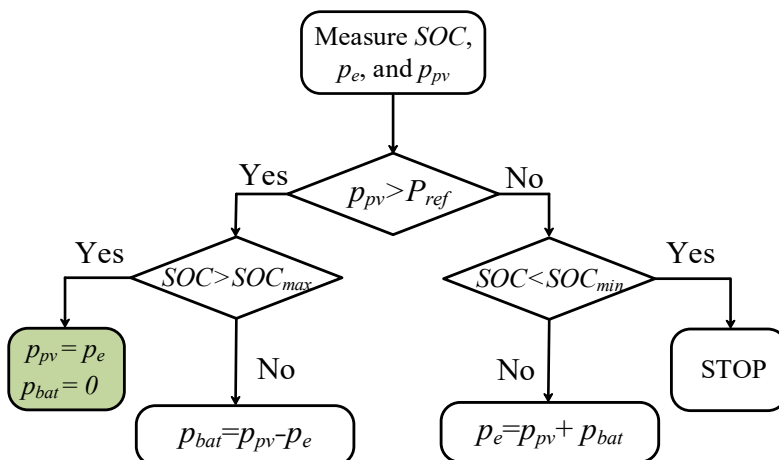


**Figure 15.** Coordinated control II for mode division and switching (PV system works at MPP or reduced power).

Moreover, due to the inherent properties of batteries, the charge/discharge rate cannot exceed specified limitations. As depicted in Figure 16, this constraint is considered in the control, as described in [87]. Coordinated control III is similar to coordinated control II, both being divided based on the SOC, PV power, and grid power demand. The principal distinction in coordinated control III is that if the battery discharge rate surpasses the permissible threshold, the batteries will sustain the maximum allowable rate. This same principle is applicable to the charging process.

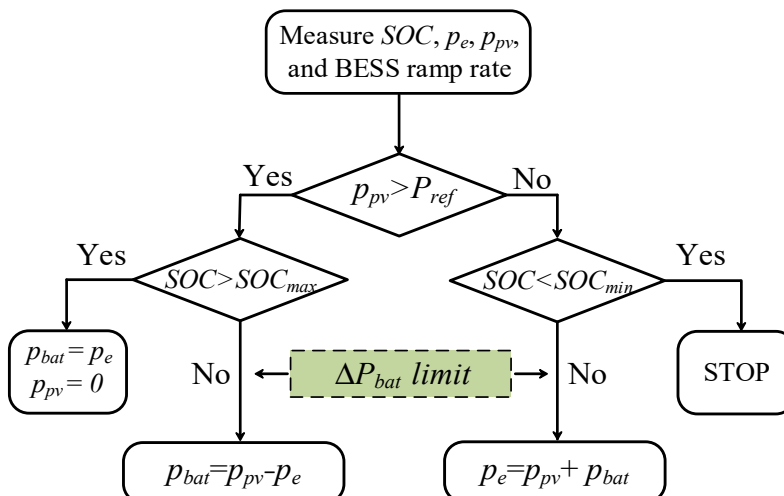


**Figure 16.** Coordinated control 2162 for mode division and switching (consider the battery ramp rate).

A more detailed PV-BES-GFM system operation mode is clarified in [88]. The operation modes are divided based on the status of the PV system, grid, and the SOC of the battery, as described in Figure 17. The control strategy encompasses scenarios where the grid provides energy to the primary source. First, whether the grid absorbs or provides power to the primary source is determined by the system operators. If the primary source is required to supply power to the grid ( $P_{ref} > 0$ ), the control strategy is identical to coordinated control II. Otherwise, the batteries act as a load to absorb the excess energy. Therefore, it is necessary to further determine whether the PV system is working or not to determine the source of the BES charging energy. If the PV system is working ( $p_{pv} \neq 0$ ), the batteries are charged to realize power balance by both the grid and the PV system with constant power. The PV system operates at a reduced power to control the DC-link voltage, and the inverter is regulated by the rectified VSG control in this mode. When the PV system is not working ( $p_{pv} = 0$ ), the batteries are only charged by the grid at constant power and the inverter is regulated by the rectified VSG control. Furthermore, the operation mode is divided according to the SOC of the battery, in alignment with the previously discussed coordinated control.

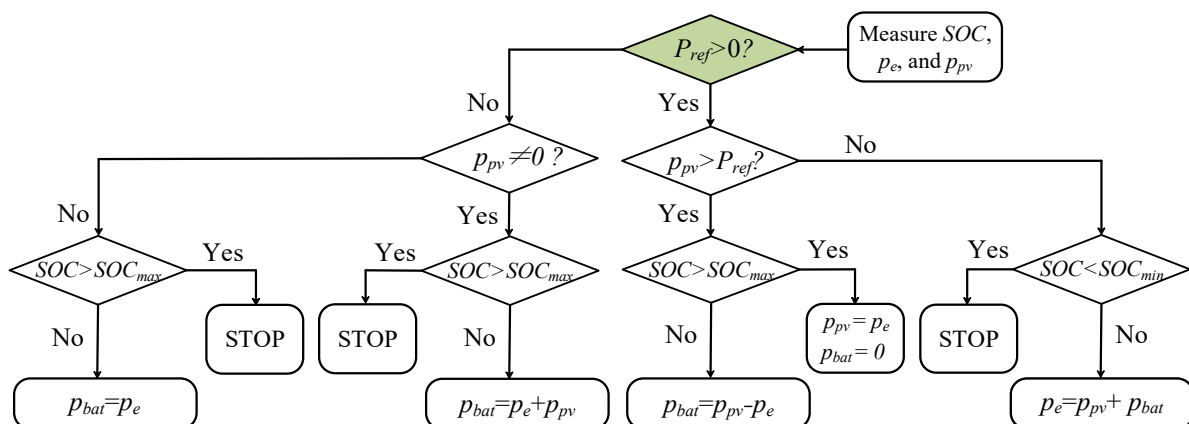


**Figure 17.** Coordinated control IV for mode division and switching (the grid provides power to the primary source).

#### 4.2. Specific Mode Switching and Division Methods

In addition to utilizing the system active power and the SOC for mode division and switching, the common DC bus configuration provides extensive degrees of freedom. This results in more flexible operation mode division and switching methods. Since both the

BES system and the PV system are integrated at the DC bus, the DC-link voltage effectively indicates the power balance within the PV-BES-GFM system. Therefore, the DC-link voltage is considered to differentiate the operations of the PV-BES system and realize mode switching [89]. As illustrated in Figure 18,  $V_{dcdown1}$  and  $V_{dcup1}$  are the lower and upper limits of the DC-link voltage under normal system operation, respectively.  $V_{dcdown2}$  and  $V_{dcup2}$  are the lower and upper limits of the additional control thresholds, respectively. This allows the DC-link voltage to fluctuate between  $V_{dcdown1}$  and  $V_{dcup1}$ , with additional control measures implemented only when the voltage exceeds the upper limit of the range.

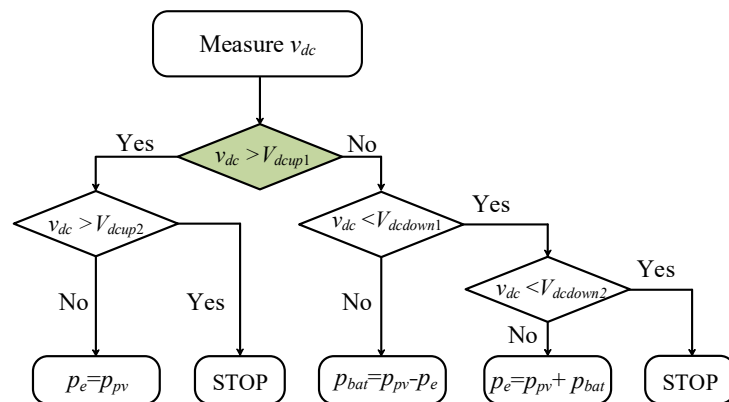


**Figure 18.** Coordinated control V for mode division and switching (employ the DC-link voltage to regulate the power flow).

When  $v_{dc}$  drops below  $V_{dcup1}$  but remains beyond  $V_{dcdown1}$ , the maximum PV power can be absorbed by the system, and the matching control is used to synchronize with the grid, enabling effective GFM control. When  $v_{dc}$  exceeds  $V_{dcup1}$ , it demonstrates that the grid and the BES are unable to absorb the maximum PV power. Consequently, the PV system operates at a reduced power to control the DC-link voltage while the GFM control becomes ineffective and is unable to provide support to the grid. However, once  $v_{dc}$  goes beyond  $V_{dcup2}$ , it indicates that the PV system has attempted to reduce PV power but has failed to regulate the DC-link voltage. Consequently, the PV-BES-GFM system will be shut down. When  $v_{dc}$  drops below  $V_{dcdown1}$  but remains beyond  $V_{dcdown2}$ , it indicates that the primary source cannot supply adequate power to the grid. The voltage difference between the  $v_{dc}$  and  $V_{dcdown1}$  is added to the matching control through a PI controller in this mode. Therefore, the DC-link voltage can be regulated at  $V_{dcdown1}$  through the droop relationship between the active power and frequency. Once  $v_{dc}$  goes below  $V_{dcdown2}$ , it shows that the maximum power of the PV system and the batteries have been transmitted to the grid. However, the DC-link voltage still cannot be regulated. The PV-BES-GFM system will be shut down. Moreover, a hysteresis comparator is adopted to avoid frequent mode switching in the PV system [90], which acts as a safe margin to prevent accidental switching. However, how to set the proper margin of the DC-link voltage remains unclear. Moreover, permitting fluctuations in the DC bus voltage can impact the operation of the PV-BES system, resulting in distortion of the inverter output voltage. The comparison of the coordinated controls in the PV-BES-GFM system is illustrated in Table 3, which highlights the key characteristics and application of each coordinated control.

**Table 3.** Comparison of the coordinated controls in the PV-BES-GFM system.

Control	Configuration	Characteristics
Coordinated control I	(1) Common AC bus connection (2) Common DC bus connection (3) TPCs	PV system always works at MPP.
Coordinated control II	(1) Common AC bus connection (2) Common DC bus connection (3) TPCs	PV system works at MPP or reduced power.
Coordinated control III	(1) Common AC bus connection (2) Common DC bus connection (3) TPCs	The battery ramp rate is considered.
Coordinated control IV	(1) Common AC bus connection (2) Common DC bus connection (3) TPCs	The scenario in which the grid supplies energy to the source has been considered.
Coordinated control V	Common DC bus connection	The DC-link voltage is employed to regulate the power flow.

#### 4.3. Coordinated Control Strategies to Improve the Power Flow Performance

In addition to mode division and switching, the power flow dynamics also need to be improved by PV-BES coordinated GFM controls to provide rapid grid voltage and frequency support. It should be noted that the BES control is critical to respond to the disturbance in the PV-BES-GFM system. Supercapacitors (SC) and batteries are suggested as a hybrid energy primary source used in [91]. The SCs are employed for instantaneous power response, while the batteries are utilized to compensate for relatively long-term and slow dynamic power fluctuations. The power fluctuation in the PV-BES-GFM system can be expressed as

$$\Delta P_b = -\frac{\Lambda f}{R_d} \cdot K_p(t), \quad (9)$$

$$\Delta P_c = -2H \frac{d\Delta f}{dt}, \quad (10)$$

where  $\Delta P_b$  and  $\Delta P_c$  represent the energy restored in batteries and supercapacitors, respectively.  $\Delta f$  represents the difference between the rated frequency and grid frequency.  $R_d$  and  $H$  represent the droop coefficient and inertia, respectively. The transfer function  $K_p(t)$  models the dynamics of the speed governor. Therefore, the power can be managed, which allocates fast-varying  $-2H \cdot d\Delta f / dt$  to the SCs and the slow-changing  $-\Delta f \cdot K_p(t) / R_d$  to the batteries. However, the cost of SCs is not desirable, and the optimal ratio of SCs to batteries in the PV-BES-GFM system remains unclear.

Additionally, an improved coordinated GFM control has been proposed in [92] to regulate the fast instantaneous and slow power flow in the PV-BES-GFM system. The active power control loop of the VSG control regulates the slow power flow. The fast instantaneous power flow is regulated by the dual voltage and current control loop controlled by the BES system. However, the dynamics of the voltage control loop are compromised by the current control loop, which affects power balance and fails to meet the requirements for a fast dynamic response. Therefore, an AC power feedforward control is proposed to improve the dynamic response of the DC-link voltage, achieving fast power balance, as shown in Figure 19. Moreover, a two-stage control strategy is proposed to improve the power flow dynamics in the PV-BES-GFM system [37]. The BES system power is manipulated in the first stage based on the grid power prediction data. In the second stage, the frequency feedback control adjusts the BES system. The BES system output power can be better managed in anticipation of frequency deviations. However, this control method depends on the grid power data and the accuracy of the prediction algorithm, which becomes more complex and unable to respond to unexpected load changes.

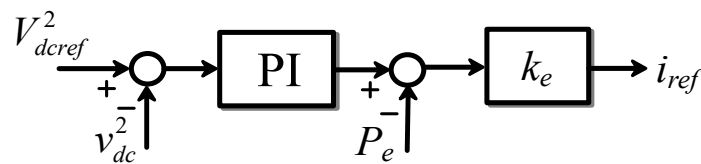


**Figure 19.** Fast instantaneous power flow control (PI: proportional integral controller;  $k$ : normalization coefficient).

#### 4.4. Challenges and Prospects of Coordinated GFM Control in PV-BES Systems

Existing mode switching methods in coordinated GFM control exhibit significant limitations, such as energy losses, high currents, and disruptive transitions, which affect PV-BESS system performance and reliability [93–97]. Achieving seamless mode transitions enhances system stability and efficiency. The transient stability during PV-BES system is also needed to be considered to ensure that the system can effectively respond to sudden changes and disturbances during mode transitions, maintaining overall stability and reliability. Additionally, it should be mentioned that the performance of the PV-BES-GFM system highly depends on the control parameters of the coordinated GFM strategies. The control parameters often rely on empirical values towards the PV-BES system in previous research, lacking design methods, which are challenging to design due to the interactions among the PV system, the BES system, and the grid-connected inverter [98]. Currently, the control parameter design is relatively mature for individual PV systems or BES systems connected to the grid. For instance, a design method has been proposed for the boost converter in PV systems [99], and the small signal model of the bi-directional DC-DC converter has been analyzed for BES systems [100]. Nevertheless, the interaction and coordination between the PV system and the BES system are not considered. The following aspects can be regarded as future directions of the PV-BES-GFM system.

- (1) Seamless mode transitions: develop coordinated control strategies to enable seamless mode transitions, minimizing power losses and transient times.
- (2) Transient stability: consider transient stability during PV-BES system mode switching.
- (3) System modeling and parameter design: model the PV-BES system and design control parameters to ensure system stability.

#### 5. Conclusions

This paper presents an overview of PV-BES systems for GFM operation based on different configurations. The typical configurations of the PV-BES systems are reviewed and categorized. By conducting a comparison of various system configurations, effective configurations such as the common DC bus topology are identified, highlighting its numerous control degrees of freedom and ease of expansion. Coordinated GFM controls are analyzed in PV-BES systems based on different configurations. Mode division and switching coordinated control based on the system active power is the most widely used. Additionally, challenges in parameter design for coordinated control strategies are addressed, with recommendations provided to enhance the efficiency and reliability of PV-BES-GFM systems.

**Author Contributions:** K.Y.: conceptualization, analysis methodology, and writing original draft; Y.X.: analysis methodology and reviewing; X.S.: provided related technical and material support; Y.Z. and Y.Y.: writing—reviewing and editing. All authors have read and agreed to the published version of the manuscript.

**Funding:** This research was funded by the National Natural Science Foundation of China under Grant 52107212 and in part by the Postdoctoral Fellowship Program of CPSF under Grant Number GZB20240644.

**Data Availability Statement:** The references analyzed in the article can be obtained at <https://www.webofscience.com/wos> and <https://ieeexplore.ieee.org/Xplore/home.jsp>.

**Conflicts of Interest:** The authors declare no conflict of interest.

## References

1. Blaabjerg, F.; Yang, Y.; Kim, K.A.; Rodriguez, J. Power electronics technology for large-scale renewable energy generation. *Proc. IEEE* **2023**, *111*, 335–355. [[CrossRef](#)]
2. Liu, Y.; You, S.; Tan, J.; Zhang, Y.; Liu, Y. Frequency response assessment and enhancement of the U.S. power grids toward extra-high photovoltaic generation penetrations—an industry perspective. *IEEE Trans. Power Syst.* **2018**, *33*, 3438–3449. [[CrossRef](#)]
3. Zhu, Y.; Wen, H.; Chu, G.; Hu, Y.; Li, X.; Ma, J. High-Performance Photovoltaic Constant Power Generation Control with Rapid Maximum Power Point Estimation. *IEEE Trans. Ind. Appl.* **2021**, *57*, 714–729. [[CrossRef](#)]
4. Blaabjerg, F.; Teodorescu, R.; Liserre, M.; Timbus, A.V. Overview of control and grid synchronization for distributed power generation systems. *IEEE Trans. Ind. Electron.* **2006**, *53*, 1398–1409. [[CrossRef](#)]
5. Pattabiraman, D.; Lasseter, R.H.; Jahns, T.M. Comparison of grid following and grid forming control for a high inverter penetration power system. In Proceedings of the 2018 IEEE Power & Energy Society General Meeting (PESGM), Portland, OR, USA, 5–10 August 2018; pp. 1–5.
6. White Paper: Grid Forming Functional Specifications for BPS-Connected Battery Energy Storage Systems. Available online: [www.nerc.com](http://www.nerc.com) (accessed on 6 June 2023).
7. Meng, X.; Liu, J.; Liu, Z. A Generalized Droop Control for Grid-Supporting Inverter Based on Comparison between Traditional Droop Control and Virtual Synchronous Generator Control. *IEEE Trans. Power Electron.* **2019**, *34*, 5416–5438. [[CrossRef](#)]
8. Qu, Z.; Peng, J.C.-H.; Yang, H.; Srinivasan, D. Modeling and Analysis of Inner Controls Effects on Damping and Synchronizing Torque Components in VSG-Controlled Converter. *IEEE Trans. Energy Convers.* **2021**, *36*, 488–499. [[CrossRef](#)]
9. Zhu, Y.; Wen, H.; Bu, Q.; Wang, X.; Hu, Y.; Chen, G. An Improved Photovoltaic Power Reserve Control with Rapid Real-Time Available Power Estimation and Drift Avoidance. *IEEE Trans. Ind. Electron.* **2023**, *70*, 11287–11298. [[CrossRef](#)]
10. Sreedevi, J.; Ashwin, N.; Raju, M.N. A study on grid connected PV system. In Proceedings of the 2016 National Power Systems Conference (NPSC), Bhubaneswar, India, 19–21 December 2016; pp. 1–6.
11. Shi, B.; Zhao, Z.; Yuan, L. A Novel Coordinated Control Strategy for Energy Storage System in DC Microgrid with Weak Communication. *IEEE Trans. Ind. Appl.* **2020**, *56*, 800–814. [[CrossRef](#)]
12. Babaei, E.; Abu-Rub, H.; Suryawanshi, H.M. Z-Source Converters: Topologies, Modulation Techniques, and Application—Part I. *IEEE Trans. Ind. Electron.* **2018**, *65*, 5092–5095. [[CrossRef](#)]
13. Alsiraji, H.A.; ElShatshat, R.; Radwan, A.A. A novel control strategy for the interlinking converter in hybrid microgrid. In Proceedings of the 2017 IEEE Power & Energy Society General Meeting, Chicago, IL, USA, 16–20 July 2017; pp. 1–5.
14. Lasseter, R.H.; Chen, Z.; Pattabiraman, D. Grid-Forming Inverters: A Critical Asset for the Power Grid. *IEEE J. Emerg. Sel. Top. Power Electron.* **2020**, *8*, 925–935. [[CrossRef](#)]
15. Luo, H.; Xiao, Y.; Zhu, Y.; Yang, Y.; Papanikolaou, N.P.; Molinas, M. A Review of Recent Requirements for Inverter-Based Resources and Grid-Forming Technologies. In Proceedings of the 2023 25th European Conference on Power Electronics and Applications (EPE'23 ECCE Europe), Aalborg, Denmark, 4–8 September 2023; pp. 1–9.
16. Liu, P.; Sun, S.; Guan, Y.; Wang, Y.; Xie, X. An overview of hybrid control strategy presenting grid-following and grid-forming capabilities. In Proceedings of the 12th International Conference on Renewable Power Generation (RPG 2023), Shanghai, China, 14–15 October 2023; pp. 567–572.
17. Rosso, R.; Wang, X.; Liserre, M.; Lu, X.; Engelken, S. Grid-Forming Converters: Control Approaches, Grid-Synchronization, and Future Trends—A Review. *IEEE Open J. Ind. Appl. IEEE Open J. Ind. Appl.* **2021**, *2*, 93–109. [[CrossRef](#)]
18. Zhao, L.; Wang, X.; Jin, Z. Flexible Synchronization Control for Grid-Forming Converters with Regulated DC-Link Dynamics. In Proceedings of the 2022 IEEE Energy Conversion Congress and Exposition (ECCE), Detroit, MI, USA, 9–13 October 2022; pp. 1–8.
19. Hazra, P.; Hadidi, R.; Makram, E. Dynamic study of virtual oscillator-controlled inverter based distributed energy source. In Proceedings of the 015 North American Power Symposium (NAPS), Charlotte, NC, USA, 4–6 October 2015; pp. 1–6.
20. Lu, M.; Dhople, S.; Johnson, B. Benchmarking Nonlinear Oscillators for Grid-Forming Inverter Control. *IEEE Trans. Power Electron.* **2022**, *37*, 10250–10266. [[CrossRef](#)]
21. Khalilpour, R.; Vassallo, A. Planning and operation scheduling of PV-battery systems: A novel methodology. *Renew. Sustain. Energy Rev.* **2016**, *53*, 194–208. [[CrossRef](#)]
22. Nottrott, A.; Kleissl, J.; Washom, B. Storage dispatch optimization for grid-connected combined photovoltaic-battery storage systems. In Proceedings of the 2012 IEEE Power and Energy Society General Meeting, San Diego, CA, USA, 22–26 July 2012; pp. 1–7.
23. Hung, D.Q.; Mithulanathan, N.; Bansal, R.C. Integration of PV and BES units in commercial distribution systems considering energy loss and voltage stability. *Appl. Energy* **2014**, *113*, 1162–1170. [[CrossRef](#)]
24. Alhatlani, A.; Batarseh, I. Review of Partially Isolated Three-Port Converters for PV-Battery Systems That Interface a PV, Bidirectional Battery, and Load. In Proceedings of the 2019 IEEE Conference on Power Electronics and Renewable Energy (CPERE), Aswan, Egypt, 23–25 October 2019; pp. 465–472.
25. Sharma, R.K.; Mudaliyar, S.; Mishra, S. Power management and economic load dispatch-based control of hybrid PV-battery-diesel standalone AC system. In Proceedings of the 2018 IEEMA Engineer Infinite Conference (eTechNxT), New Delhi, India, 13–14 March 2018; pp. 1–6.
26. Narayanan, V.; Kewat, S.; Singh, B. Control and Implementation of a Multifunctional Solar PV-BES-DEGS Based Microgrid. *IEEE Trans. Ind. Electron.* **2021**, *68*, 8241–8252. [[CrossRef](#)]

27. Naqvi, S.B.Q.; Singh, B. Weak Grid Integrated Improved Power Quality PV-Battery System with Controlled Power Flow and Grid Assistive Capabilities. *IEEE Trans. Ind. Appl.* **2024**, *60*, 4517–4529. [[CrossRef](#)]
28. Mitali, J.; Dhinakaran, S.; Mohamad, A.A. Energy storage systems: A review. *Energy Storage Sav.* **2022**, *1*, 166–216. [[CrossRef](#)]
29. Choi, J.; Lee, J.I.; Lee, I.W.; Cha, S.W. Robust PV-BESS Scheduling for a Grid with Incentive for Forecast Accuracy. *IEEE Trans. Sustain. Energy* **2022**, *13*, 567–578. [[CrossRef](#)]
30. Joshi, J.; Swami, A.K.; Jately, V.; Azzopardi, B. A Comprehensive Review of Control Strategies to Overcome Challenges During LVRT in PV Systems. *IEEE Access* **2021**, *9*, 121804–121834. [[CrossRef](#)]
31. Yang, X.; Ren, J.; Li, X. Slope Control Method with Variable Coefficients of Battery Energy Storage System for Smoothing Photovoltaic Power Fluctuation. *Autom. Electr. Power Syst.* **2016**, *40*, 56–63.
32. Mishra, J.; Behera, P.K.; Pattnaik, M.; Samanta, S. An Efficient Supervisory Power Management Scheme for a Wind–Battery-Assisted Hybrid Autonomous System. *IEEE Syst. J.* **2023**, *17*, 768–779. [[CrossRef](#)]
33. Liu, J.; Hou, Y.; Guo, J.; Liu, X.; Liu, J. A Cost-Efficient Virtual Synchronous Generator System Based on Coordinated Photovoltaic and Supercapacitor. *IEEE Trans. Power Electron.* **2023**, *38*, 16219–16229. [[CrossRef](#)]
34. Qian, Z.; Abdel-Rahman, O.; Hu, H.; Batarseh, I. An integrated three-port inverter for stand-alone PV applications. In Proceedings of the 2010 IEEE Energy Conversion Congress and Exposition, Atlanta, GA, USA, 12–16 September 2010; pp. 1471–1478.
35. Zhang, Z.; Fang, J.; Dong, C.; Jin, C.; Tang, Y. Enhanced Grid Frequency and DC-Link Voltage Regulation in Hybrid AC/DC Microgrids Through Bidirectional Virtual Inertia Support. *IEEE Trans. Ind. Electron.* **2023**, *70*, 6931–6940. [[CrossRef](#)]
36. Gupta, Y.; Amin, M. Adaptive Droop Controller for PV—Battery Based Microgrids. In Proceedings of the 2022 IEEE Energy Conversion Congress and Exposition (ECCE), Detroit, MI, USA, 9–13 October 2022; pp. 1–6.
37. Rajabinezhad, M.A.; Guerrero, J.M. A Three-Level Control Strategy for Battery Energy Storage System to Mitigate Power fluctuations and Compensate Reactive Power of Distributed Generators in a Microgrid. In Proceedings of the 2020 10th Smart Grid Conference (SGC), Kashan, Iran, 16–17 December 2020; pp. 1–6.
38. Mahmood, H.; Blaabjerg, F. Autonomous Power Management of Distributed Energy Storage Systems in Islanded Microgrids. *IEEE Trans. Sustain. Energy* **2022**, *13*, 1507–1522. [[CrossRef](#)]
39. Al-Obaidi, N.A.; Abbas, R.A.; Khazaal, H.F. A Review of Non-Isolated Bidirectional DC-DC Converters for Hybrid Energy Storage System. In Proceedings of the 2022 5th International Conference on Engineering Technology and its Applications (IICETA), Al-Najaf, Iraq, 31 May–1 June 2022; pp. 248–253.
40. Lithesh, G.; Krishna, B.; Karthikeyan, V. Review and Comparative Study of Bi-Directional DC-DC Converters. In Proceedings of the 2021 IEEE International Power and Renewable Energy Conference (IPRECON), Kollam, India, 24–26 September 2021; pp. 1–6.
41. Kanaparthi, R.K.; Singh, J.P.; Ballal, M.S. A Review on Multi-Port Bidirectional Isolated and Non-Isolated DC-DC Converters for Renewable Applications. In Proceedings of the 2022 IEEE International Conference on Power Electronics, Drives and Energy Systems (PEDES), Jaipur, India, 14–17 December 2022; pp. 1–6.
42. Yang, S.; Shoyama, M.; Zaitsu, T.; Yamamoto, J.; Abe, S.; Ninomiya, T. Detail operating characteristics of Bi-directional LLC resonant converter. In Proceedings of the 2012 International Conference on Renewable Energy Research and Applications (ICRERA), Nagasaki, Japan, 11–14 November 2012; pp. 1–6.
43. Kim, E.-S.; Park, J.-H.; Jeon, Y.-S.; Kong, Y.-S.; Lee, S.-M.; Kim, K. Bidirectional secondary LLC resonant converter using auxiliary switches and inductor. In Proceedings of the 2014 IEEE Applied Power Electronics Conference and Exposition—APEC 2014, Fort Worth, TX, USA, 16–20 March 2014; pp. 1941–1947.
44. Doncker, R.W.D.; Divan, D.M.; Kheraluwala, M.H. A three-phase soft-switched high power density DC/DC converter for high power applications. *IEEE Trans. Ind. Appl.* **1991**, *27*, 63–73. [[CrossRef](#)]
45. Shao, S.; Chen, L.; Shan, Z.; Gao, F.; Chen, H.; Sha, D.; Dragičević, T. Modeling and Advanced Control of Dual-Active-Bridge DC-DC Converters: A Review. *IEEE Trans. Power Electron.* **2022**, *37*, 1524–1547. [[CrossRef](#)]
46. Qin, H.; Kimball, J.W. Generalized Average Modeling of Dual Active Bridge DC–DC Converter. *IEEE Trans. Power Electron.* **2012**, *27*, 2078–2084.
47. Tavakoli, S.D.; Kadkhodaei, G.; Mahdavyfakhr, M.; Hamzeh, M.; Sheshyekani, K. Interlinking converters in application of bipolar dc microgrids. In Proceedings of the 2017 8th Power Electronics, Drive Systems & Technologies Conference (PEDSTC), Mashhad, Iran, 14–16 February 2017; pp. 37–42.
48. Peng, F.Z. Z-source inverter. *IEEE Trans. Ind. Appl.* **2003**, *39*, 504–510. [[CrossRef](#)]
49. Peng, F.Z. Z-source inverter. In Proceedings of the IAS Annual Meeting, Pittsburgh, PA, USA, 13–18 October 2002; Volume 2, pp. 775–781.
50. Nguyen, M.-K.; Jung, Y.-G.; Lim, Y.-C. Single-Phase AC–AC Converter Based on Quasi-Z-Source Topology. *IEEE Trans. Power Electron.* **2010**, *25*, 2200–2210. [[CrossRef](#)]
51. Nguyen, M.-K.; Lim, Y.-C.; Cho, G.-B. Switched-Inductor Quasi-Z-Source Inverter. *IEEE Trans. Power Electron.* **2011**, *26*, 3183–3191. [[CrossRef](#)]
52. Vinnikov, D.; Roasto, I. Quasi-Z-Source-Based Isolated DC/DC Converters for Distributed Power Generation. *IEEE Trans. Ind. Electron.* **2011**, *58*, 192–201. [[CrossRef](#)]
53. Liang, W.; Liu, Y.; Shen, Y. Active Power Control Integrated with Reactive Power Compensation of Battery Energy Stored Quasi-Z Source Inverter PV Power System Operating in VSG Mode. *IEEE J. Emerg. Sel. Top. Power Electron.* **2023**, *11*, 339–350. [[CrossRef](#)]

54. Tang, Z.; Yang, Y.; Blaabjerg, F. An interlinking converter for renewable energy integration into hybrid grids. *IEEE Trans. Power Electron.* **2021**, *36*, 2499–2504. [[CrossRef](#)]
55. Sun, D.; Du, L.; Lu, X.; He, L. An Energy-Stored Quasi-Z Source Converter Based Interlinking Converter for Hybrid AC/DC Microgrids. In Proceedings of the IECON 2018—44th Annual Conference of the IEEE Industrial Electronics Society, Washington, DC, USA, 21–23 October 2018; pp. 3821–3826.
56. Wang, L.; Lee, M.-F.; Zhang, C.-D.; Lin, J.-J.; Tseng, C.-C. Frequency Control of a Bidirectional Interlinking Converter in an Islanded Hybrid AC/DC Microgrid. In Proceedings of the 2022 IET International Conference on Engineering Technologies and Applications (IET-ICETA), Changhua, Taiwan, 14–16 October 2022; pp. 1–2.
57. Bose, U.; Chattopadhyay, S.; Chakraborty, C. Topological investigation on interlinking converter in a hybrid microgrid. In Proceedings of the 2018 IEEE International Conference on Industrial Electronics for Sustainable Energy Systems (IESES), Hamilton, New Zealand, 31 January–2 February 2018; pp. 62–67.
58. Hema, V.K.; Dhanalakshmi, R. Operation of hybrid AC-DC microgrid with an interlinking converter. In Proceedings of the 2014 IEEE International Conference on Advanced Communications, Control and Computing Technologies, Ramanathapuram, India, 8–10 May 2014; pp. 38–42.
59. Huang, L.; Xin, H.; Wang, Z.; Zhang, L.; Wu, K.; Hu, J. Transient stability analysis and control design of droop-controlled voltage source converters considering current limitation. *IEEE Trans. Smart Grid* **2019**, *10*, 578–591. [[CrossRef](#)]
60. Zhu, Y.; Wen, H.; Chu, G.; Wang, X.; Peng, Q.; Hu, Y.; Jiang, L. Power-Rating Balance Control and Reliability Enhancement in Mismatched Photovoltaic Differential Power Processing Systems. *IEEE Trans. Power Electron.* **2022**, *37*, 879–895. [[CrossRef](#)]
61. Singhal, A.; Vu, T.L.; Du, W. Consensus Control for Coordinating Grid-Forming and Grid-Following Inverters in Microgrids. *IEEE Trans. Smart Grid* **2022**, *13*, 4123–4133. [[CrossRef](#)]
62. Mejbaul, M.H.; Wolfs, P.J.; Alahakoon, S.; Islam, M.A.; Nadarajah, M.; Zare, F.; Omar, F. Three-Port Converters for Energy Conversion of PV-BES Integrated Systems—A Review. *IEEE Access* **2023**, *11*, 6551–6573.
63. Ling, Y.; Li, Y.; Yang, Z.; Xiang, J. A Dispatchable Droop Control Method for Distributed Generators in Islanded AC Microgrids. *IEEE Trans. Ind. Electron.* **2021**, *68*, 8356–8366. [[CrossRef](#)]
64. Sun, Y.; Hou, X.; Yang, J.; Han, H.; Su, M.; Guerrero, J.M. New Perspectives on Droop Control in AC Microgrid. *IEEE Trans. Ind. Electron.* **2017**, *64*, 5741–5745. [[CrossRef](#)]
65. Eajal, A.A.; Yazdavar, A.H.; El-Saadany, E.F.; Salama, M.M.A. Optimizing the Droop Characteristics of AC/DC Hybrid Microgrids for Precise Power Sharing. *IEEE Syst. J.* **2021**, *15*, 560–569. [[CrossRef](#)]
66. Majumder, R.; Chaudhuri, B.; Ghosh, A.; Majumder, R.; Ledwich, G.; Zare, F. Improvement of Stability and Load Sharing in an Autonomous Microgrid Using Supplementary Droop Control Loop. *IEEE Trans. Power Syst.* **2010**, *25*, 796–808. [[CrossRef](#)]
67. Vasquez, J.C.; Guerrero, J.M.; Savaghebi, M.; Eloy-Garcia, J.; Teodorescu, R. Modeling, Analysis, and Design of Stationary-Reference-Frame Droop-Controlled Parallel Three-Phase Voltage Source Inverters. *IEEE Trans. Ind. Electron.* **2013**, *60*, 1271–1280. [[CrossRef](#)]
68. Zhong, Q.C.; Weiss, G. Synchronverters: Inverters That Mimic Synchronous Generators. *IEEE Trans. Ind. Electron.* **2011**, *58*, 1259–1267. [[CrossRef](#)]
69. Li, D.; Zhu, Q.; Lin, S.; Bian, X.Y. A Self-Adaptive Inertia and Damping Combination Control of VSG to Support Frequency Stability. *IEEE Trans. Energy Convers.* **2017**, *32*, 397–398. [[CrossRef](#)]
70. Wang, Q.; Zhou, D.; Yin, S.; Lei, Y.; He, T. Improved Adaptive Inertia and Damping Coefficient Control Strategy of VSG Based on Optimal Damping Ratio. In Proceedings of the 2022 International Power Electronics Conference (IPEC-Himeji 2022- ECCE Asia), Himeji, Japan, 15–19 May 2022; pp. 102–107.
71. Dhople, S.V.; Johnson, B.B.; Hamadeh, A.O. Virtual Oscillator Control for voltage source inverters. In Proceedings of the 2013 51st Annual Allerton Conference on Communication, Control, and Computing (Allerton), Monticello, IL, USA, 2–4 October 2013; pp. 1359–1363.
72. Johnson, B.B.; Dhople, S.V.; Hamadeh, A.O.; Krein, P.T. Synchronization of Nonlinear Oscillators in an LTI Electrical Power Network. *IEEE Trans. Circuits Syst. I Regul. Pap.* **2014**, *61*, 834–844. [[CrossRef](#)]
73. Lu, M. Virtual Oscillator Grid-Forming Inverters: State of the Art, Modeling, and Stability. *IEEE Trans. Power Electron.* **2022**, *37*, 11579–11591. [[CrossRef](#)]
74. Lu, M.; Dutta, S.; Purba, V.; Dhople, S.; Johnson, B. A grid-compatible virtual oscillator controller: Analysis and design. In Proceedings of the 2019 IEEE Energy Conversion Congress and Exposition (ECCE), Baltimore, MD, USA, 29 September–3 October 2019; pp. 2643–2649.
75. Johnson, B.B.; Sinha, M.; Ainsworth, N.G.; Dörfler, F.; Dhople, S.V. Synthesizing virtual oscillators to control islanded inverters. *IEEE Trans. Power Electron.* **2016**, *31*, 6002–6015. [[CrossRef](#)]
76. Gurugubelli, V.; Ghosh, A.; Panda, A.K.; Behera, B.P. Fuzzy-Based Adaptive VOC Methods for Parallel Inverters. *IEEE Trans. Power Electron.* **2024**, *39*, 3956–3961. [[CrossRef](#)]
77. Arghir, C.; Dörfler, F. The Electronic Realization of Synchronous Machines: Model Matching, Angle Tracking, and Energy Shaping Techniques. *IEEE Trans. Power Electron.* **2020**, *35*, 4398–4410. [[CrossRef](#)]
78. Zhao, L.; Jin, Z.; Wang, X. Small-Signal Synchronization Stability of Grid-Forming Converters with Regulated DC-Link Dynamics. *IEEE Trans. Ind. Electron.* **2023**, *70*, 12399–12409. [[CrossRef](#)]

79. Zhao, L.; Wang, X.; Jin, Z. Impedance-Based Dynamics Analysis for DC-Link Voltage-Synchronized Voltage-Source Converters. *IEEE Trans. Power Electron.* **2023**, *38*, 10829–10844. [[CrossRef](#)]
80. Zhang, L.; Harnefors, L.; Nee, H.-P. Power-Synchronization Control of Grid-Connected Voltage-Source Converters. *IEEE Trans. Power Syst.* **2010**, *25*, 809–820. [[CrossRef](#)]
81. Mahmood, H.; Michaelson, D.; Jiang, J. Decentralized power management of a PV/battery hybrid unit in a droop-controlled islanded microgrid. *IEEE Trans. Power Electron.* **2015**, *30*, 7215–7229. [[CrossRef](#)]
82. Yang, Y.; Qin, Y.; Tan, S.; Hui, S.Y.R. Efficient improvement of photovoltaic-battery systems in standalone dc microgrids using a local hierarchical control for the battery system. *IEEE Trans. Power Electron.* **2019**, *34*, 10796–10807. [[CrossRef](#)]
83. Merabet, A.; Ahmed, K.T.; Ibrahim, H.; Beguenane, R.; Ghias, A.M.Y.M. Energy management and control system for laboratory scale microgrid based wind-PV-battery. *IEEE Trans. Sustain. Energy* **2017**, *8*, 145–154. [[CrossRef](#)]
84. Tofighi, A.; Kalantar, M. Power management of PV/battery hybrid power source via passivity-based control. *Renew. Energy* **2011**, *36*, 2440–2450. [[CrossRef](#)]
85. Zhou, H.; Bhattacharya, T.; Tran, D.; Siew, T.S.T.; Khambadkone, A.M. Composite Energy Storage System Involving Battery and Ultracapacitor with Dynamic Energy Management in Microgrid Applications. *IEEE Trans. Power Electron.* **2011**, *26*, 923–930. [[CrossRef](#)]
86. Li, D.; Ho, C.N.M. Decentralized PV-BES Coordination Control with Improved Dynamic Performance for Islanded Plug-Play DC Microgrid. *IEEE J. Sel. Top. Power Electron.* **2021**, *9*, 4992–5001. [[CrossRef](#)]
87. Wang, L.; Bai, F.; Yan, R.; Saha, T.K. Real-Time Coordinated Voltage Control of PV Inverters and Energy Storage for Weak Networks with High PV Penetration. *IEEE Trans. Power Syst.* **2018**, *33*, 3383–3395. [[CrossRef](#)]
88. Yin, K.; Xiao, Y.; Yang, Y. A Coordinated PV-Battery GFM Control for Power Management and Frequency Support. In Proceedings of the 2023 IEEE 2nd International Power Electronics and Application Symposium (PEAS), Guangzhou, China, 10–13 November 2023; pp. 797–802.
89. Liu, Y.; Wang, Y.; Wang, M.; Xu, Z.; Peng, Y.; Li, M. Coordinated VSG Control of Photovoltaic/Battery System for Maximum Power Output and Grid Supporting. *IEEE J. Emerg. Sel. Top. Circuits Syst.* **2022**, *12*, 301–309. [[CrossRef](#)]
90. Mao, M.; Qian, C.; Ding, Y. Decentralized coordination power control for islanding microgrid based on PV/BES-VSG. *IEEE CPSS* **2018**, *3*, 14–24. [[CrossRef](#)]
91. Fang, J.; Tang, Y.; Li, H.; Li, X. A Battery/Ultracapacitor Hybrid Energy Storage System for Implementing the Power Management of Virtual Synchronous Generators. *IEEE Trans. Power Electron.* **2018**, *33*, 2820–2824. [[CrossRef](#)]
92. Quan, X.; Yu, R.; Zhao, X.; Lei, Y.; Chen, T.; Li, C.; Huang, A.Q. Photovoltaic Synchronous Generator: Architecture and Control Strategy for a Grid-Forming PV Energy System. *IEEE J. Emerg. Sel. Top. Power Electron.* **2020**, *8*, 936–948. [[CrossRef](#)]
93. Tafti, H.; Townsend, C.D.; Farivar, G.; Sangwongwanich, A.; Yang, Y.; Pou, J.; Blaabjerg, F. Extended Functionalities of Photovoltaic Systems With Flexible Power Point Tracking: Recent Advances. *IEEE Trans. Power Electron.* **2020**, *35*, 9342–9356. [[CrossRef](#)]
94. Zhu, Y.; Wen, H.; Tafti, H.D.; Wang, G.; Bu, Q.; Chu, G.; Shi, H.; Hu, Y.; Jiang, L. Novel Fast-Speed Partial-Shading-Tolerant Flexible Power Point Tracking for Photovoltaic Systems With Explicit Key Points Estimation. *IEEE Trans. Sustain. Energy* **2024**, *15*, 466–485. [[CrossRef](#)]
95. Shukl, P.; Singh, B. Dual Mode Operation of PV-BES Based Microgrid with Seamless Transition Capability. In Proceedings of the 2021 IEEE 2nd International Conference on Smart Technologies for Power, Energy and Control (STPEC), Bilaspur, Chhattisgarh, India, 19–22 December 2021; pp. 1–6.
96. Kanchev, H.; Lu, D.; Colas, F.; Lazarov, V.; Francois, B. Energy Management and Operational Planning of a Microgrid With a PV-Based Active Generator for Smart Grid Applications. *IEEE Trans. Ind. Electron.* **2011**, *58*, 4583–4592. [[CrossRef](#)]
97. Riffonneau, Y.; Bacha, S.; Barruel, F.; Ploix, S. Optimal Power Flow Management for Grid Connected PV Systems with Batteries. *IEEE Trans. Sustain. Energy* **2011**, *2*, 309–320. [[CrossRef](#)]
98. Sun, K.; Zhang, L.; Xing, Y.; Guerrero, J.M. A Distributed Control Strategy Based on DC Bus Signaling for Modular Photovoltaic Generation Systems with Battery Energy Storage. *IEEE Trans. Power Electron.* **2011**, *26*, 3032–3045. [[CrossRef](#)]
99. Ashtiani, N.A.; Azizi, S.M.; Khajehoddin, S.A. Robust Control Design for High-Power Density PV Converters in Weak Grids. *IEEE Trans. Control Syst. Technol.* **2019**, *27*, 2361–2373. [[CrossRef](#)]
100. Wu, F.; Fan, S.; Luo, S. Small-Signal Modeling and Closed-Loop Control of Bidirectional Buck-Boost Current-Fed Isolated DC-DC Converter. *IEEE Trans. Ind. Electron.* **2021**, *68*, 4036–4045. [[CrossRef](#)]

**Disclaimer/Publisher’s Note:** The statements, opinions and data contained in all publications are solely those of the individual author(s) and contributor(s) and not of MDPI and/or the editor(s). MDPI and/or the editor(s) disclaim responsibility for any injury to people or property resulting from any ideas, methods, instructions or products referred to in the content.